JOURNAL OF MATERIALS SCIENCE 28 (1993) 1578–1584

Effect of cold rolling on the elastic properties of $(Al_2O_3)_p$–Al composite

J. C. LEE, K. N. SUBRAMANIAN
Department of Metallurgy, Mechanics and Materials Science, Michigan State University, East Lansing, MI 48824-1226, USA.

Mechanical shaping of an aluminium alloy reinforced with Al_2O_3 particulates, $(Al_2O_3)_p$–Al, was carried out by a cold rolling operation. Rolling was performed unidirectionally in a direction perpendicular to the extrusion direction of the composite, until edge cracks formed. Cold rolling was found to cause particulate cracking and interfacial debonding, as well as the redistribution of $(Al_2O_3)_p$. These parameters have significant roles in determining the elastic properties of the resultant composite.

1. Introduction

Metal-matrix composites reinforced with ceramic particulates, due to their improved mechanical properties, their economy of fabrication, and the ease of mechanical shaping, are gaining commercial importance for potential applications such as engine components [1–5], structural [6, 7] and aerospace [8, 9] materials. However, these applications involve mechanical working during the shaping process. The mechanical forces associated with mechanical working not only cause redistribution of the reinforcements, but also cause microscopic damage such as particulate cracking and interfacial debonding [10], affecting the material properties of the resultant composite. Changes in mechanical properties, especially elastic properties, due to mechanical shaping are one of the important considerations that have to be taken into account in engineering design.

The elastic modulus is usually measured from the slope of the proportional region in the stress–strain diagram. However, this property can also be measured very accurately using the sonic resonance method, with minimal error due to inelastic behaviour. The principal idea behind this method can be explained using the equation by which one can measure the propagating speed of a sonic wave through a medium. For flexural waves travelling through a solid

$$f \propto (E/\rho)^{1/2} \quad (1)$$

where f is the frequency of the flexural wave, E the elastic modulus of the solid and ρ the density of the solid. The elastic modulus of a solid material is proportional to its density and the squared value of the flexural resonance frequency. Therefore, if the resonance frequency of a material can be measured, the elastic modulus can be calculated. This method is often called the "sonic resonance method" or "dynamic resonance technique".

The objectives of the present study are to investigate the effect of cold rolling on the redistribution of $(Al_2O_3)_p$ clusters and microcracks in $(Al_2O_3)_p$–Al composites, and to study their influences on the elastic properties of the resultant composites.

2. Experimental procedure

2.1. Specimen preparation

Duralcan composite (W6A 10A) with 6061 aluminium alloy reinforced with 10 vol % of $(Al_2O_3)_p$, obtained in the form of extruded cylindrical bar with extrusion ratio of 20:1, was used in this study. A three-dimensional view of as-extruded composite, exhibiting banding of $(Al_2O_3)_p$ clusters along the direction of extrusion, is shown in Fig. 1. The size of $(Al_2O_3)_p$ was measured using an optical image analyser and found to have an average major dimension of 9.6 μm with an aspect ratio of about 2.

The stock material was cut out, annealed at 560 °C for 30 min, and quenched in cold water before rolling. Cold rolling was carried out unidirectionally to various percentages of reduction in thickness in a direction perpendicular (transverse) to the extruded

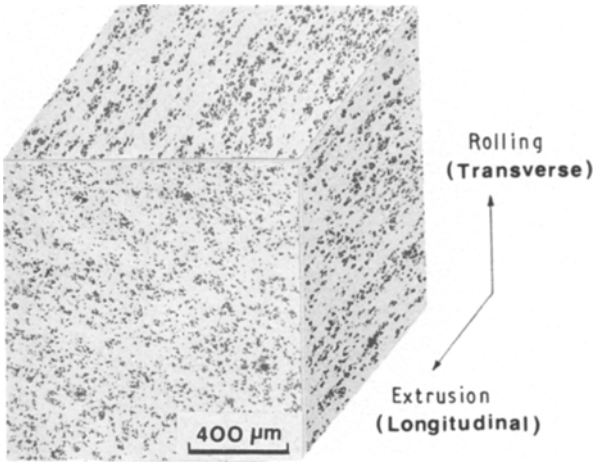

Figure 1 A three-dimensional view of as-extruded $(Al_2O_3)_p$–Al composite exhibiting banding of $(Al_2O_3)_p$ clusters along the direction of extrusion.

0022–2461

direction. A reduction ratio of about 10% per pass was used to obtain homogeneous matrix flow. Thin slices with a direction parallel (longitudinal) and perpendicular (transverse) to the extruded direction were cut from the rolled sheets with a low-speed diamond saw. These slices were polished with abrasive papers and rotating laps in order to remove the damaged surface layer affected by rolls. Prismatic bars with dimensions of 46.85 mm × 9.1 mm × 0.95 mm were machined from these slices.

As-received and cold-rolled specimens annealed at different temperatures were etched with Keller's reagent to reveal the grain boundaries. The grain size measurements on these specimens were performed using the line intercept method. The grain sizes of heavily rolled composites are found to be generally smaller than those of the lightly rolled ones [11, 12]. However, the influence of annealing temperature on the resultant grain size was more significant than that of the amount of prior cold work (Fig. 2a and b). As a result, two different solution treatment temperatures have to be selected to obtain the same grain size in specimens subjected to different extents of cold work. The details of T6 heat treatments used are

(i) solution treatment: 560 °C for 1 h (for as-received composite), 590 °C for 1 h (for all cold-rolled composites);

(ii) room-temperature ageing for 65 h; and

(iii) artificial ageing: 170 °C for 14 h (to obtain peak hardness).

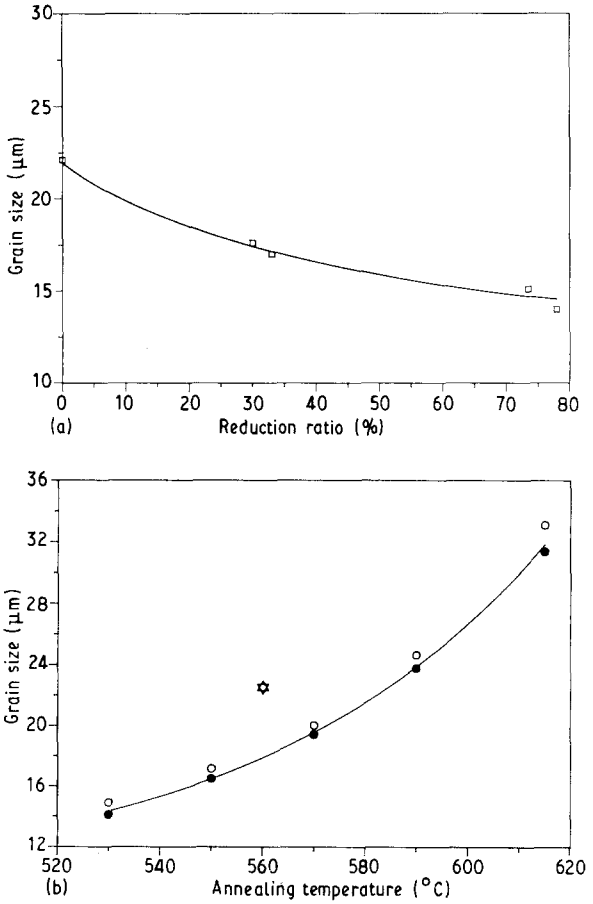

Figure 2 Measurements of the grain size of the composite as a function of (a) amount of prior cold rolling (annealed at 560°C for 1 h) and (b) annealing temperature: (✡) as received, (○) 32% rolled, (●) 78% rolled.

An average grain size of about 23 μm in the peak hardness condition was obtained for all the specimens used for elastic modulus measurements.

2.2. Test procedure

All measurements of elastic modulus were carried out at room temperature in air using the standard sonic resonance test method designated by ASTM C848-78. All specimens were suspended by cotton threads by attaching them to points located at a distance (15% of the specimen length) from the two ends of the prismatic bar-shaped specimens so as to minimize possible experimental errors in the elastic modulus measurements caused by shifts in the location of the supporting threads.

3. Background for elastic modulus measurement

The measurements of elastic modulus consist of matching the oscillator frequency with mechanical resonance vibration of the specimen. Both fundamental flexural and torsional resonance frequencies were measured for the specimens which were cold-rolled into different reduction ratios and subjected to T6 treatment. Using the measured weight and dimensions of the specimens, the elastic and shear modulus can be calculated from the flexural and torsional resonance frequencies, respectively.

The equation used for calculation of the elastic modulus is that for prisms of rectangular cross-section provided by Pickett [13]. For the fundamental mode of vibration

$$E = 0.94642\left(\frac{l^4}{t^2}\right)\rho f^2 T \tag{2}$$

where E = elastic modulus, l = length of the specimen, t = thickness of the specimen, ρ = density of the specimen, f = fundamental flexural resonance frequency and T = shape factor which depends on the shape of the specimen. T is given approximately by [14]

$$T = \left[1 + 6.585(1 + 0.0752\nu + 0.8109\nu^2)\left(\frac{t}{l}\right)^2 - 0.868\left(\frac{t}{l}\right)^4\right] - \left[\frac{8.34(1 + 0.2023\nu + 2.173\nu^2)(t/l)^4}{1 + 6.338(1 + 0.14081\nu + 1.536\nu^2)(t/l)^2}\right] \tag{3}$$

where ν = Poisson's ratio. The shear modulus can also be calculated by determining the torsional resonance frequency. The basic equation which relates torsional resonance frequency with shear modulus is [13]

$$G = \left(\frac{2l}{n}\right)^2 \rho f'^2 R \tag{4}$$

where G = shear modulus, n = an integer which is unity for the fundamental mode (2 for the first overtone etc.), f' = torsional resonance frequency and R = shape factor which depends on the shape of the

specimen. For prisms of rectangular cross-section, the best approximation for R was obtained by Spinner and Tefft [15]:

$$R = R_0\left[1 + 0.0085\left(\frac{nb}{l}\right)^2\right] - 0.06\left(\frac{nb}{l}\right)^{3/2}\left(\frac{b}{a} - 1\right)^2 \quad (5)$$

where b = width of the specimen, a = thickness of the specimen and

$$R_0 = \left[\frac{1 + (b/a)^2}{4 - 2.521\,(a/b)\{1 - 1.991/[\exp(\pi b/a) + 1]\}}\right] \quad (6)$$

Poisson's ratio (v) can be obtained from measured values of E and G.

4. Results

4.1. Effect of rolling on microstructure

Cold rolling was carried out on as-extruded composites, until edge cracks were observed on the specimens, to study the effects of mechanical working on the size and redistribution of $(Al_2O_3)_p$ clusters in these composites. Although 10% of reduction in thickness per pass was used, the composite could be rolled up to about 75% of reduction in thickness without edge cracking or surface scuffing. During cold rolling, the hardness of the composite increases rapidly with increasing reduction ratio, as shown in Fig. 3. The rolled sheets of composite were cut and examined with SEM. A significant amount of particulate cracking and interfacial debonding were observed on the polished surfaces, as shown in Fig. 4. There was a strong tendency for the crack planes to be parallel to the direction of compression (i.e. rolling pressure) and to be perpendicular to the rolling direction (i.e. feed direction) as can be seen in Fig. 5. Grid analysis performed on micrographs taken from the rolled composite showed that the number of damaged $(Al_2O_3)_p$ particles increased linearly with increasing reduction ratio as illustrated in Fig. 6. The substantial increase in rolling pressure, which is caused by the increase in hardness of the composite during cold rolling, was considered to be

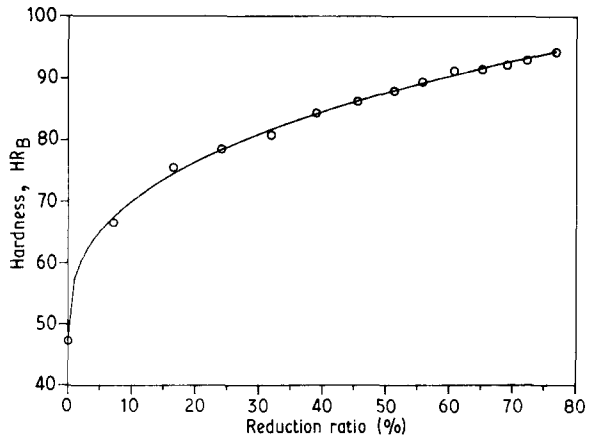

Figure 3 Plot of hardness of the cold-rolled composite as a function of reduction ratio.

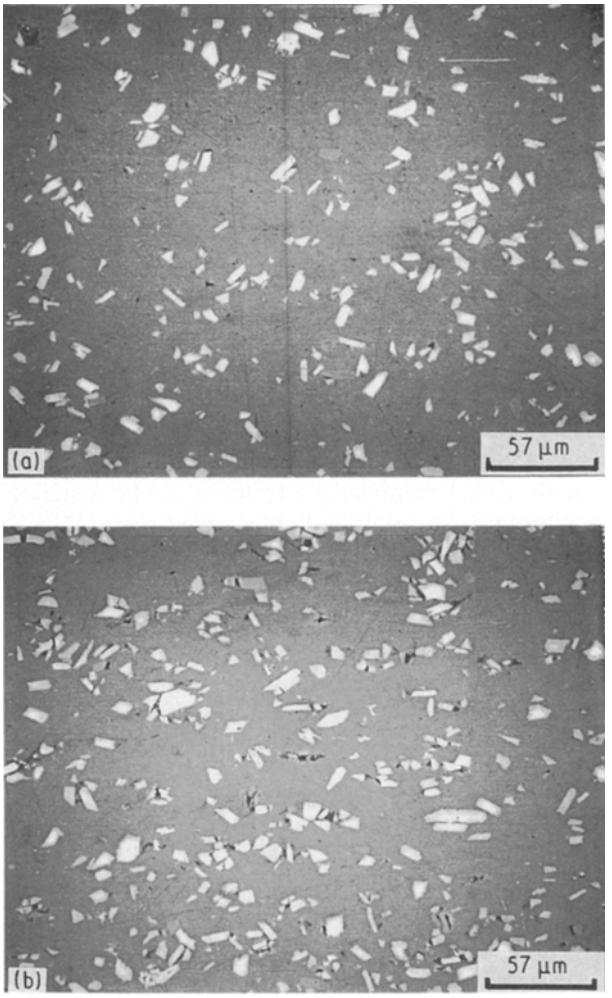

Figure 4 SEM micrographs of (a) as-extruded (0%) and (b) 60% cold-rolled composites. Note that 60% cold-rolled composite exhibits a significant amount of interfacial debonding and particulate cracking, while almost no crack damage can be seen on the as-extruded composite.

responsible for such cracking and debonding in the composites.

A considerable change in the distribution and shape of the $(Al_2O_3)_p$ clusters could be observed in the rolled composites. The most apparent difference in metallographic features between the as-extruded and the rolled composites is that the $(Al_2O_3)_p$, initially present in the form of banded clusters in as-extruded composite, becomes more uniformly distributed with increasing percentage of reduction. The banded clusters of $(Al_2O_3)_p$ in the composite almost disappear at about 70% reduction, as can be observed in the micrographs presented in Fig. 7.

4.2. Effect of rolling on elastic properties

Considerable increases in elastic modulus (about 18% for both L and T directions) and shear modulus (about 15–20% depending on the direction) were measured in as-extruded 6061 Al alloy reinforced with 10% of $(Al_2O_3)_p$. The elastic modulus measured along the transverse direction of as-extruded composite (transverse elastic modulus) was found to be slightly higher than that along the longitudinal direction (longitudinal elastic modulus). The transverse shear

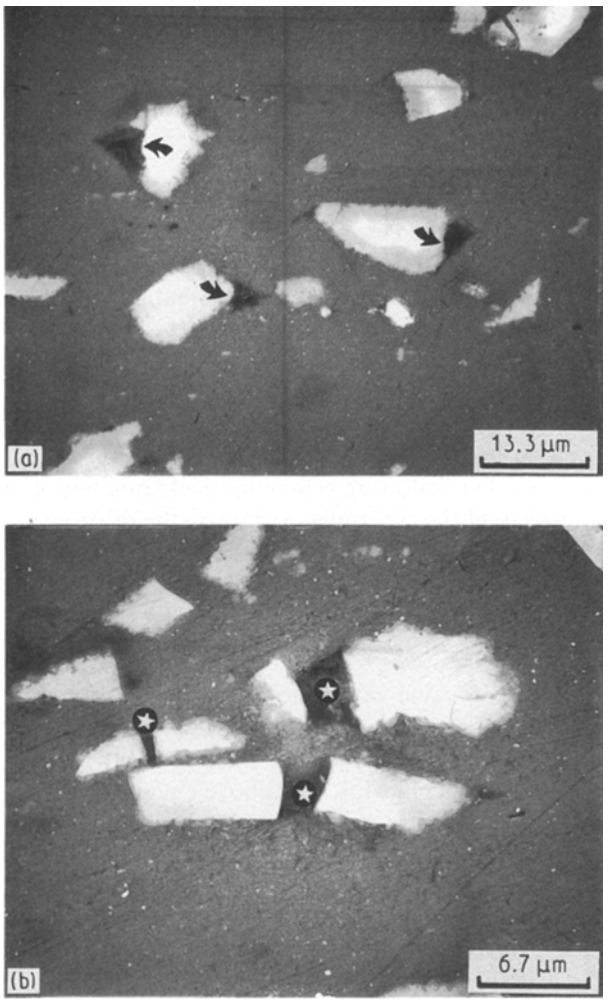

Figure 5 SEM micrographs illustrating (a) interfacial debonding (arrows) and (b) particulate cracking (☆). Note that crack planes are oriented perpendicular to the rolling direction.

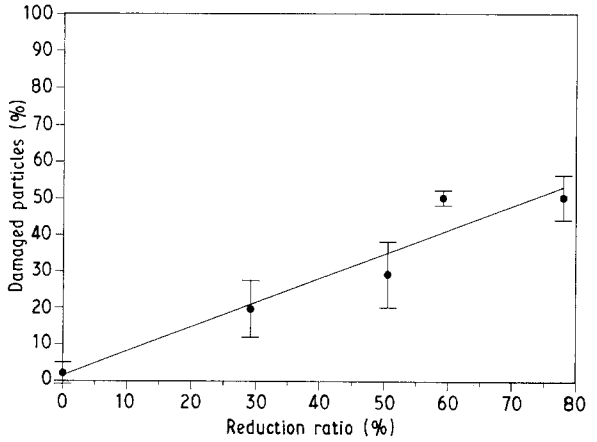

Figure 6 Plot of the percentage of damaged $(Al_2O_3)_p$ as a function of reduction ratio.

modulus was also higher than the longitudinal shear modulus. Some typical values of E, G and ν of the unreinforced 6061-Al alloy and the as-received (as-extruded) composite are compared in Table I.

The measured values of E, G and ν as a function of reduction ratio are listed in Table II, and are plotted in Fig. 8. As illustrated in Fig. 8a, the longitudinal elastic modulus was observed to increase significantly at the

Figure 7 Optical micrographs exhibiting the distribution of $(Al_2O_3)_p$ clusters in (a) as-extruded and (b) 75% cold-rolled composite.

TABLE I Comparison of E, G and ν between unreinforced 6061 Al alloy and as-extruded composite, under T6 heat-treated conditions

Material	Direction[a]	E (GPa)	G (GPa)	ν
6061 Al alloy	All	68.0	25.6	0.33
10% $(Al_2O_3)_p$–Al	L	79.9	30.2	0.323
	T	80.7	31.7	0.274

[a]All : random direction, L : longitudinal direction, T : transverse direction.

TABLE II Variation in the elastic properties of 10% $(Al_2O_3)_p$–Al composite as a function of reduction ratio (values obtained from the best-fit curve)[a]

Reduction ratio (%)	E (GPa)		G (GPa)		ν	
	L	T	L	T	L	T
0	79.9	80.7	30.2	31.7	0.32	0.27
10	81.2	81.1	30.7	31.8	0.33	0.28
20	83.4	81.1	31.0	31.8	0.34	0.28
30	83.8	80.7	31.2	31.8	0.34	0.27
40	83.5	80.2	31.2	31.6	0.34	0.27
50	82.9	79.6	31.1	31.5	0.33	0.26
60	82.2	79.0	30.8	31.3	0.33	0.26
70	81.6	78.7	30.5	31.2	0.33	0.26

[a]T: transverse direction, L: longitudinal direction.

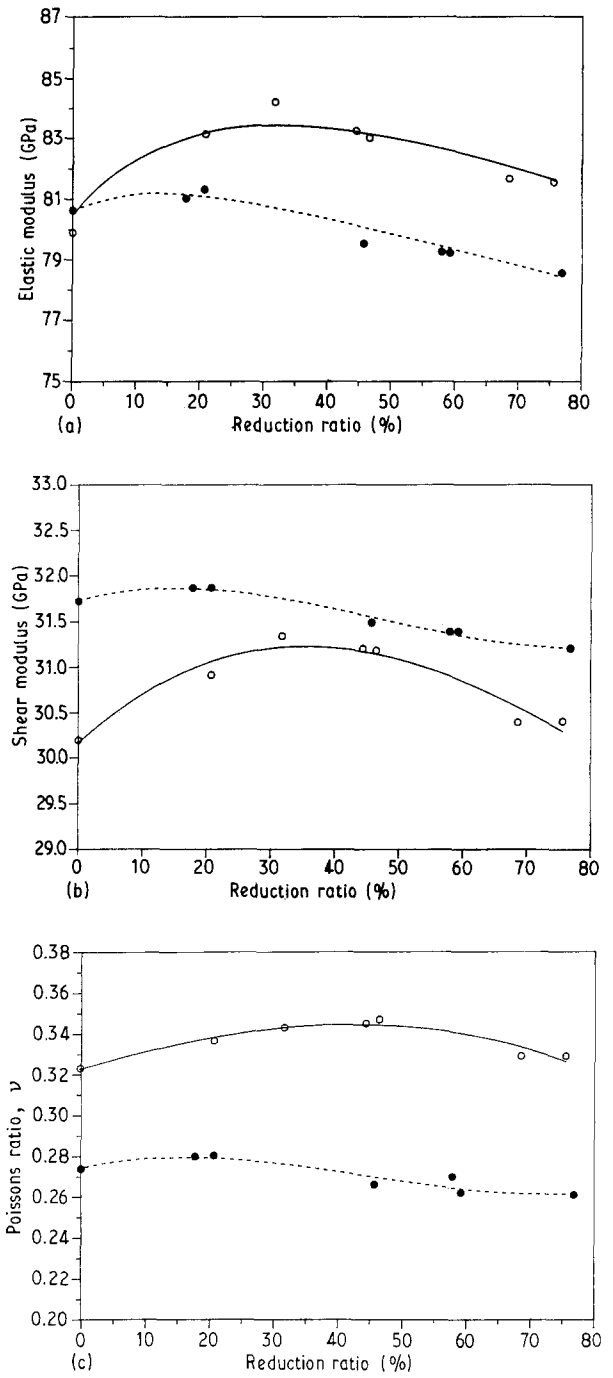

Figure 8 Plots of experimentally obtained E, G and ν as a function of reduction ratio along (○) longitudinal and (●) transverse directions. All specimens were T6 treated before measurements. (a) Elastic modulus, (b) shear modulus, (c) Poisson's ratio.

early stages of cold rolling, and decrease afterwards. Nevertheless, the elastic modulus remains higher than that of as-extruded composite even after 70% of reduction. However, the transverse elastic modulus increases slightly at the early stages of cold rolling, and decreases afterwards.

The transverse elastic modulus becomes lower than that of as-extruded composite after about 30% of reduction. Such features could also be observed for the shear modulus and Poisson's ratio measured with respect to reduction ratio, as shown in Fig. 8b and c.

The shear modulus was found to be always higher along the transverse direction than along the longitudinal direction, even after rolling. However, the elastic modulus was found to be higher along the longitudinal direction than along the transverse direction except at very small amounts of cold work: hence, under a given elastic stress the rolled composites should undergo less tensile deformation along the longitudinal direction, and less shear deformation along the transverse direction.

5. Discussion

5.1. Effect of porosity on the elastic properties

A quantitative assessment of the effect of porosity on various material properties such as thermal conductivity, elastic properties etc. has been carried out extensively in brittle materials, such as glass, ceramics etc. [16–18]. The following semi-empirical equations can be used to fit the experimental data on the relationship between elastic properties and porosity:

$$U = U_0(1 - \alpha P) \quad (7a)$$

$$U = U_0 \exp(-\beta P) \quad (7b)$$

where U_0 = value of elastic properties of pore-free material, U = value of elastic properties of material with porosity, P = the volume fraction of pore and α, β = empirical constants. The above equations illustrate that the elastic properties of solid materials decrease with increasing volume percentage of porosity. They vary linearly for small (a few per cent) volume percentages of porosity. A schematic illustration of such a relationship is shown in Fig. 9a.

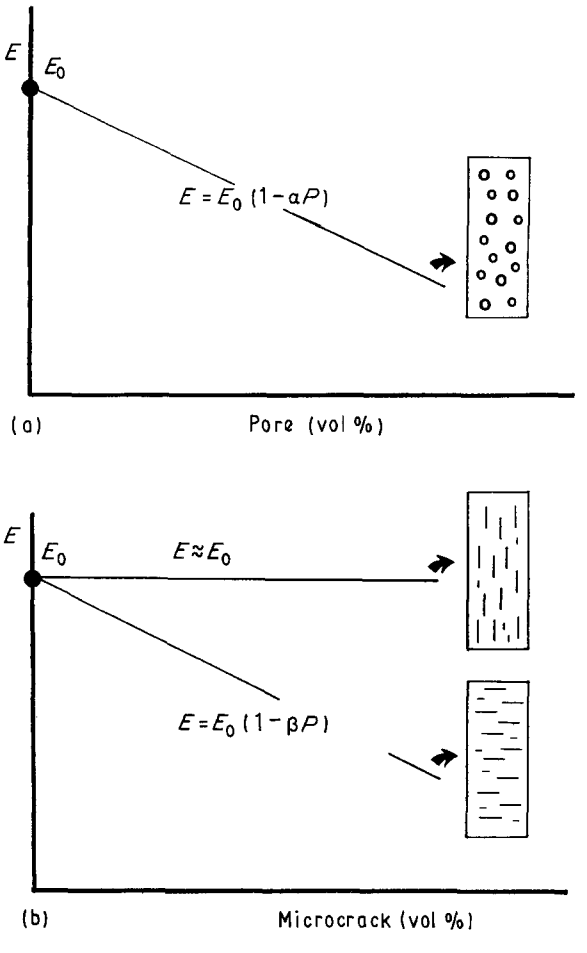

Figure 9 Schematic diagrams illustrating the effect of (a) porosity and (b) microcracking on the material properties.

5.2. Effect of microcracks on the elastic properties

A theoretical analysis of the effect of microcracks on various material properties such as thermal conductivity, thermal stress resistance, elastic properties etc. has also been well established in the field of brittle materials [19–21]. According to Hasselman and Singh [19], the relative effect of microcracking on a given material property, Q_0, can be given in the general form

$$Q = Q_0[1 - \eta] \quad \text{or} \quad Q = Q_0[1 + \eta]^{-1} \tag{8}$$

where Q_0 = value of the material property of crack-free material, Q = value of the material property of microcracked material, and η = a function of Poisson's ratio of crack-free material (ν_0), crack density, and crack shape.

The same expression can be used to investigate the effect of microcracking on the elastic properties. For a material having microcracks with crack planes oriented perpendicular to the uniaxial tension, the elastic modulus can be obtained by using the equation [21]

$$E = E_0[1 - F(\nu_0)\Phi] \tag{9}$$

where E = elastic modulus of microcracked material, E_0 = elastic modulus of crack-free material, $F(\nu_0)$ = a function of Poisson's ratio, depending on the shape of the microcrack (e.g. $F(\nu_0) = 16(1 - \nu_0^2)/3$ for penny-shaped cracks), ν_0 = Poisson's ratio of crack-free material, and Φ = crack density parameter given by $\Phi = (2N/\pi)(A^2/P)$ where N = density of crack (mm^{-3}), A = crack area per crack and P = perimeter per crack.

However, for a material having microcracks with crack planes oriented parallel to the uniaxial tension, the elastic modulus of cracked material will almost be the same as that of crack-free material [19]. In other words, the propagation of a sonic wave is not impeded by a parallel crack. Thus

$$E \simeq E_0 \tag{10}$$

As a summary, during uniaxial tensile loading the elastic modulus is not influenced by microcracks oriented parallel to the direction of loading, but is affected by microcracks oriented perpendicular to the loading direction. Schematic illustrations of such features are given in Fig. 9b.

5.3. Effect of cold rolling on the elastic properties

Although cold rolling results in the uniform distribution of $(Al_2O_3)_p$ clusters with increasing reduction ratio (Fig. 7), it does induce elliptical pore-like microcracks with crack planes oriented perpendicular to the rolling direction (Fig. 5). Such pore-like microcracks include particulate cracks and interfacial debonding which can be considered as both crack and pore. In the present discussion, the effect of redistribution of $(Al_2O_3)_p$ and pore-like microcracks on the variation of the elastic properties of the composite, especially the elastic modulus, will be considered.

Since the crack planes of microcracks developed within a transverse specimen are oriented perpendicular to the tensile direction, the transverse elastic modulus of rolled composites will decrease due to pore-like microcracks according to Equation 9. However, the effect of such microcracks on the longitudinal elastic modulus will not be as significant as that on the transverse ones, since the crack planes are oriented parallel to the direction of the propagating wave. On the other hand, the redistribution of $(Al_2O_3)_p$ achieved by rolling is considered to be attributable to the increase in both the longitudinal and transverse elastic modulus due to the fine dispersion of $(Al_2O_3)_p$ and break-up of clusters. Analytical expressions concerning the contribution of the two parameters to the elastic modulus can be obtained from curve-fitting of the data points for the transverse specimens under the following assumptions:

(a) Only the redistribution and the microcracks of $(Al_2O_3)_p$ act as influencing factors for the changes in elastic modulus, and

(b) The orientation of each $(Al_2O_3)_p$ particle in the longitudinal and transverse specimens does not affect the elastic modulus of the composite.

The best-fit curve for the experimentally measured values of elastic moduli was found to have the form

$$E^{\text{eff}} = E_0(1 + \alpha x^{\beta})(1 - \gamma x) \tag{11}$$

where E^{eff} = effective elastic modulus of the composite, E_0 = elastic modulus of as-extruded composite, x = reduction ratio related to the volume percentage of pore-like microcrack, and α, β, γ = constants to be determined from experimental data.

In this equation, $E_0(1 + \alpha x^{\beta})$ corresponds to the contribution due to the redistribution of $(Al_2O_3)_p$, and $(1 - \gamma x)$ corresponds to the effect due to pore-like microcracks. The contribution due to the pore-like microcracks is more significant in the transverse direction, as illustrated in Fig. 10. This is to be expected, based on the orientation of the microcracks (introduced by cold work) relative to the tensile direction. As a result, the transverse elastic modulus of cold-rolled composite is smaller than the longitudinal elastic modulus. If the damage to $(Al_2O_3)_p$ could be eliminated efficiently during rolling, the rolling operation could result in an increase in the elastic modulus of the composite according to $E^{\text{eff}} = E_0(1 + \alpha x^{\beta})$, due to the breaking up of banding and clustering so as to provide a uniform distribution of $(Al_2O_3)_p$.

6. Summary

The following statements summarize the results of cold rolling carried out on extruded $(Al_2O_3)_p$–Al composite.

6.1. Microstructural features

Significant redistribution of the $(Al_2O_3)_p$ clusters could be achieved with increasing reduction ratio by cold rolling. The composite could be rolled down to as

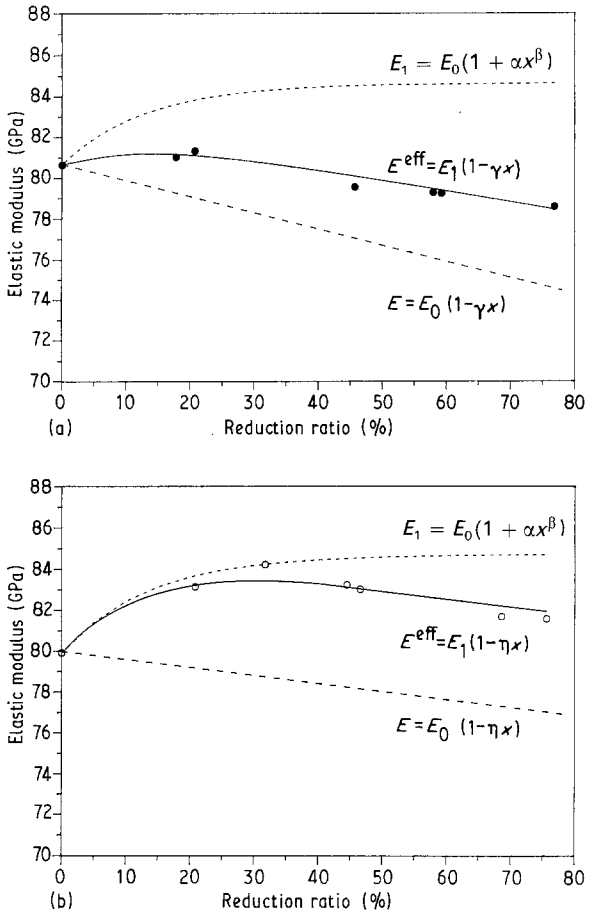

Figure 10 Plots of analytical expressions for the effects of (---) redistribution of $(Al_2O_3)_p$ and (--) pore-like microcracks on the elastic moduli along (a) transverse and (b) longitudinal directions of the composites; (●, ○) data points. Note that the effect of pore-like microcracks on the elastic modulus is less significant in the longitudinal than in the transverse direction.

much as 75% of reduction in thickness without forming any edge crackings or surface scuffings, indicating good formability. The banded structure of $(Al_2O_3)_p$ clusters present in the extruded composite almost disappeared beyond about 60–70% of reduction. Both particulate cracking and interfacial debonding were observed in the rolled composite. There is a strong tendency for crack planes to be formed perpendicular to the rolling direction. The extent of such damage in $(Al_2O_3)_p$ increases linearly with increasing reduction ratio.

6.2. Elastic properties

The measured elastic modulus and shear modulus of as-extruded composite were considerably higher than those of the unreinforced Al alloy. Although the longitudinal elastic modulus of cold-rolled composite was higher than the transverse one, the shear modulus was found to be always higher along the transverse direction than along the longitudinal direction. Both redistribution of $(Al_2O_3)_p$ and pore-like microcracks were found to affect the elastic properties of the composite. Analytical expressions which account for the contribution of both parameters to the elastic properties were obtained by using a curve-fitting method; the effect of pore-like microcracks on the elastic modulus was found to be in the form of $E^{eff} = E_0(1 - \gamma x)$, and the effect of redistribution of $(Al_2O_3)_p$ on the elastic modulus has the form $E^{eff} = E_0(1 + \alpha x^\beta)$, where x and E_0 represent the reduction ratio and elastic modulus of as-extruded composites, respectively.

Acknowledgements

The authors thank Mr Stephen Holcomb at Duralcan Co. for providing the materials used in this study. They also wish to thank Professor E.D. Case of Michigan State University and Dr Youngman Kim of Iowa State University for their valuable help and discussions.

References

1. D. R. FLINN, "The New Materials Society" Vol. 2 (Bureau of Mines, Washington D. C., 1990) p. 6.1.
2. T. W. CHOU, A. KELLY and A. OKURA, *Composite* **16** (1985) 187.
3. C. F. LEWIS, *Mater. Eng.* **103** (1986) 33.
4. J. C. BITTENCE, *Adv. Mater. Process.* **131** (1987) 39.
5. S. R. LAMPMAN, *ibid.* **138** (1991) 17.
6. H. OHTSU, in Proceedings of 5th Annual ASM/EDS Advanced Composites Conference, Detroit, Michigan, October 1989 (ASM International, Materials Park, Ohio 1989) p. 187.
7. K. MARSDEN, *J. Metals* **37** (1985) 59.
8. T. R. PRITCHETT, *Light Metal Age* **44** (1986) 10.
9. K. S. RAVICHANDRAN and E. S. DWARAKADASA, *J. Metals* **39** (1987) 28.
10. J. C. LEE and K. N. SUBRAMANIAN, in Proceedings of 6th Annual ASM/EDS Advanced Composites Conference, Detroit, Michigan, October 1990 (ASM International, Materials Park, Ohio) p.575.
11. F. N. RHINES and B. R. PATTERSON, *Metall. Trans. A* **13** (1982) 985.
12. H. L. WALKER, University of Illinois Engineering Experiment Station Bulletin No. 359 (University of Illinois, 1945).
13. G. PICKETT, *Amer. Soc. Testa Mater. Proc.* **45** (1945) 846.
14. S. SPINNER, T. W. REICHARD and W. E. TEFFT, *J. Res. Natl Bur. Stand.* **64A** (1960) 147.
15. S. SPINNER and W. E. TEFFT, *Amer. Soc. Testg Mater. Proc.* **61** (1961) 1221.
16. V. D. KRSTIC and W. H. ERICKSON, *J. Mater. Sci.* **22** (1987) 2881.
17. S. K. DUTTA, A. K. MUKHOPADHYAY and D. CHAKRABORTY, *J. Amer. Ceram. Soc.* **71** (1988) 942.
18. H. M. CHOU and E. D. CASE, *J. Mater. Sci. Lett.* **7** (1988) 1217.
19. D. P. H. HASSELMAN and J. P. SINGH, *Amer. Ceram. Soc. Bull.* (1979) 856.
20. H. J. SIEBENECK, J. J. CLEVELAND, D. P. H. HASSELMAN and R. C. BRADT, *J. Amer. Ceram. Soc.* **60** (1977) 336.
21. B. BUDIANSKY and R. J. O' CONNELL, *Int. J. Solids* **12** (1976) 81.

Received 6 November 1991
and accepted 14 August 1992